REVIEW

Dissociation Dynamics of Energy-Selected Ions with Threshold Photoelectron-Photoion Coincidence Velocity Imaging†

Xiang-kun Wu[a], Xiao-feng Tang[b], Xiao-guo Zhou[a*], Shi-lin Liu[a*]

a. Hefei National Laboratory for Physical Sciences at the Microscale, iChEM (Collaborative Innovation Center of Chemistry for Energy Materials), Department of Chemical Physics, University of Science and Technology of China, Hefei 230026, China

b. Laboratory of Atmospheric Physico-Chemistry, Anhui Institute of Optics and Fine Mechanics, Chinese Academy of Sciences, Hefei 230031, China

(Dated: Received on November 18, 2018; Accepted on December 13, 2018)

Threshold photoelectron-photoion coincidence (TPEPICO) is a powerful method to prepare and analyze internal energy- or state-selected ions. Here, we review the state-of-the-art TPEPICO imaging technique combining with tunable vacuum ultraviolet (VUV) synchrotron radiation and its recent applications at Hefei Light Source (HLS), especially on the fundamental data measurement and the dissociation dynamics of ions. By applying the double velocity map imaging for both electrons and ions in coincidence, the collection efficiency of the charged particles, the electron energy resolution and the resolving power of the released kinetic energy in dissociation have been greatly improved. The kinetic energy and the angular distributions of fragment ions dissociated from parent ions with definitive internal energy or state have been acquired directly from TPEPICO images. Some dissociation mechanisms involving non-adiabatic quantum effects, like conical intersection and internal conversion, have been revealed. Moreover, the mass-selected threshold photoelectron spectroscopy (MS-TPES) shows tremendous advantages in isomer-specific analysis of complex systems.

Key words: Photodissociation, Photoionizaiton, Coincidence, Velocity imaging

I. INTRODUCTION

Gas-phase photoionization as a fundamental photon-matter process in nature has attracted extensive attentions in the past decades. Fundamental data such as ionization energy (IE), dissociation energy (D_0) and appearance energy (AP_0) of fragment, together with the reaction dynamics, involved in the photoionization and/or dissociative photoionization processes have been measured precisely. These data as well as reaction dynamics have provided valuable information in the research fields of astrochemsitry, combustion, atmosphere chemistry and quantum information [1, 2].

Among various analytical techniques, since 1980s, with the rapid development of commercial ultraviolet (UV) lasers, the laser-based resonance enhanced multi-photon ionization (REMPI) and pump-probe methods have been often used to prepare ions in specific ionic states and investigate their spectroscopy and dissociation dynamics [3−6]. However, it is mainly used for small molecules due to an essential prerequisite of Rydberg intermediate state with a long lifetime. As the IEs of most organic molecules locate in the vacuum ultraviolet (VUV) energy range, VUV single photon ionization is considered to be universal to get internal energy-selected molecular ions. The methods of photoelectron spectroscopy (PES) and photoionization mass spectrometry (PIMS) especially combined with modern light sources such as VUV laser and synchrotron radiation have made considerable progresses to probe molecular photoionization. Synchrotron radiation taking the characters of high flux, wide energy range and continuous tenability *etc.* in the VUV range has been utilized as an ideal light source in photoionization.

By scanning synchrotron radiation in photoionization, the various electronic and vibrational states of molecular ion can be prepared as illustrated by the following equation.

$$E_{\text{ion}} = h\nu - \text{IE} - E_{\text{electron}} \quad (1)$$

where $h\nu$ is the photon energy, E_{ion} is the internal energy of ion, and E_{elecrton} is the kinetic energy of electron. Based on the principle, the electron and ion produced in the same photoionization event can be analyzed simultaneously and correlated in coincidence. Building on the capabilities of PES and

†Dedicated to Professor Kopin Liu on the occasion of his 70th birthday.

*Authors to whom correspondence should be addressed. E-mail: xzhou@ustc.edu.cn, slliu@ustc.edu.cn

PIMS, the method of photoelectron-photoion coincidence (PEPICO) spectroscopy can provide complementary information in photoionization experiments [2].

As a powerful method to prepare and analyze state-selected ions, PEPICO has been applied for a long time. In 1967, Brehm and Puttkamer [7] firstly applied PEPICO to investigate photoionization of methanol. From then on, the electron-ion coincidence measurement has been developed rapidly. A number of chemical systems including diatomic and triatomic molecules [8, 9], complex chemical systems like combustion [10, 11], clusters [12] and biomolecules [13, 14], have already been investigated. However, the electron energy resolution and the collection efficiencies for either charged particle are low in early PEPICO measurements [15]. A higher electron energy resolution can be achieved with the threshold photoelectron-photoion coincidence spectroscopy (TPEPICO) [16], in which only electrons with near zero kinetic energy, so-called threshold photoelectrons, are detected in coincidence with ions by employing a tunable light source. In the early TPEPICO investigations, many electrostatic energy analyzers, *e.g.* 127° energy analyzer [17], steradiancy analyzer [18] and hemispheric energy analyzer [19], were used to analyze photoelectron under a relatively high-intensity extraction field. Moreover, a penetrating field was also applied to improve the electron energy resolution [20]. But the balance between electron energy resolution and collection efficiency was unsatisfactory. The performance of TPEPICO has been improved with combination of velocity map imaging (VMI) of the charged particles. In 2003, Bare and Li [21] firstly applied the VMI technique to collect photoelectrons. The threshold electron energy resolution was notably improved, and the collection solid angle of photoelectrons was increased to almost 4π sr. [21]. Through optimizing the focus electric field, Garcia *et al.* [22] improved the electron energy resolution to an amazing level of less than 1 meV at SOLEIL.

Although the electron collection efficiency and the electron energy resolution were improved, the Wiley-McLaren linear TOF or reflectron TOF mass spectrometers [23] were usually utilized to measure ion. The kinetic energy release distribution (KERD) of fragment ion in dissociative photoionization was only derived from evaluation by fitting the TOF profile [3, 24−26] and hence the resolving power of kinetic energy distribution of fragment ion was very limited. Moreover, the angular distribution of fragment could not be obtained. In 2009, a double VMI was firstly used in TPEPICO measurement at Hefei Light Source (HLS) [27]. It is known that the released kinetic energy and angular distributions of fragments from the dissociation of a state-selected ion can be measured directly from the velocity imaging [28 29, 30]. Therefore, the fundamental data including IE, D_0 and AP_0 have been re-measured with high accuracy, and some detailed dissociation mechanisms of the quantum state-selected ion have been revealed [31−39]. Moreover, by scanning the VUV photon energy the mass-selected threshold photoelectron spectrum (MS-TPES) corresponding to a specific ion can be recorded. MS-TPES is regarded as a powerful tool to identify the reactive intermediates and free radicals, especially to distinguish isomers [40, 41].

This review will provide a brief introduction of TPEPICO imaging technique, and then focus on its recent progresses of application at HLS. Based on the reported results, the advantages of TPEPICO imaging technique are clearly shown, and then some new directions with VUV ionization to interrogate complex chemical systems are proposed.

II. TPEPICO VMI TECHNIQUE

A. Principle of TPEPICO

When a molecule absorbs a VUV photon with higher energy than its IE, it will be ionized. The parent ions with specific internal energy can be prepared by selecting the coincident ones with the threshold electrons, according to the energy conservation of Eq.(1). If the photon energy is beyond AP_0, a dissociative photoionization process may occur as illuminated by the following equation.

$$\mathrm{AB} + h\nu \rightarrow \mathrm{AB}^+ + \mathrm{e} \rightarrow \mathrm{A}^+ + \mathrm{B} + \mathrm{e} \tag{2}$$

Then the conservation of energy becomes a little complex and follows the equation below.

$$E_{\mathrm{AB}} + h\nu - \mathrm{IE(AB)} = E_{\mathrm{in}}(\mathrm{A}^+) + E_{\mathrm{in}}(\mathrm{B}) + E_{\mathrm{tran}} + E_{\mathrm{electron}} + D_0(\mathrm{AB}^+) \tag{3}$$

where E_{AB} is the internal energy of neutral molecule and can be ignored in supersonic molecular beam condition, $E_{\mathrm{in}}(\mathrm{A}^+)$ and $E_{\mathrm{in}}(\mathrm{B})$ are the internal energies of ion fragment and neutral fragment, respectively, E_{tran} is the total released kinetic energy in dissociation, E_{tran}=$E_{\mathrm{tran}}(\mathrm{A}^+)$+$E_{\mathrm{tran}}(\mathrm{B})$, E_{electron} is the kinetic energy of electron, and $D_0(\mathrm{AB}^+)$ is the dissociation energy of ion.

Taking into account the conservation of momentum in dissociative photoionization, $E_{\mathrm{tran}}(\mathrm{A}^+)/E_{\mathrm{tran}}(\mathrm{B})$ equals the inverse ratio of their masses, $m_{\mathrm{B}}/m_{\mathrm{A}^+}$, and thus the total translation energy distribution, E_{tran}, can be obtained from the measured kinetic energy of fragment ion. Based on the assignment of the velocity image, the internal energy distributions of fragments can be determined too. Finally, $D_0(\mathrm{AB}^+)$ can be accurately calculated with Eq.(3) in TPEPICO measurement. Moreover, the dissociation dynamics of internal energy-selected molecular ion can be investigated by measuring the kinetic energy and angular distributions of fragment ion, with the aid of high-level theoretical calculations on potential energy surfaces of low-lying electronic ionic states.

DOI:10.1063/1674-0068/32/cjcp1811257

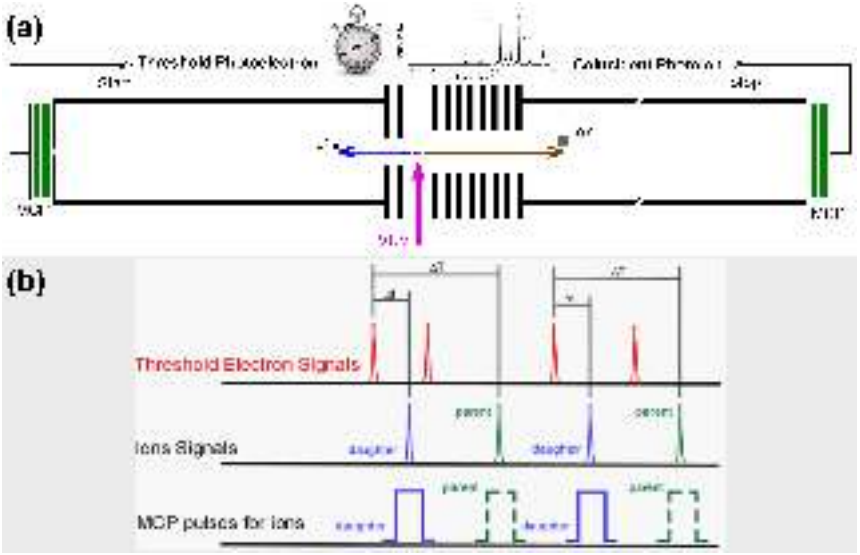

FIG. 1 (a) Schematic diagram of the time-coincident measurement at HLS. (b) Single-start/multiple-stop data acquisition mode for collecting electrons and ions under the low ionization rate (less than 1 kHz).

Generally, in a TPEPICO setup, the photoelectron often needs a few ten nanoseconds to reach the detector from photoionization region under the action of electric field, and thus it can be ignored when counting the ion flight time (usually in a few ten microseconds). Thus, when the same dc electronic field is applied for the extraction region of the TPEPICO setup, the flight time interval between the electron and the ion produced from the same photoionization event is kept constant. Based on the principle, a special time-coincidence counting mode has been developed [21], which is usually classified to two types according to the ionization rates. The triggerless multiple-start multiple-stop measurement mode is applied in Swiss Light Source (SLS) [42] and SOLEIL at France [43] according to the recording rate of threshold electrons over 100 kHz. Whilst, at HLS the single-start/multiple-stop data acquisition [27] has been used in the low ionization rate (less than 1 kHz). In this scheme, the threshold electrons provide the start signals to measure the TOFs of ions, as shown schematically in FIG. 1. A counter (FAST Comtec, Germany, P7888) records the relative time of every "stop" ion signals. An advantage of the P7888 counter is that it automatically neglects any new start signal and records all ion stop signals during the selected time circle. Therefore, the signals of true coincident ions are augmented at a certain range of flight time, while the false coincident ions (correlated to the energetic electrons) are distributed randomly. In addition, when the photoionization cross section to yield threshold photoelectrons is small, the signal-to-noise ratio becomes too worse to measure the kinetic energy and angular distributions of fragment ions. The case occurs occasionally, especially for the molecular ion in a highly excited electronic state.

B. Details of TPEPICO velocity map imaging at HLS

In TPEPICO experiment of dissociative photoionization, the most important characters are the collection efficiency, the energy resolution of threshold electrons, and the resolving power of kinetic energy distribution of fragment ion.

In the TPEPICO investigations at HLS, we usually collect photoelectrons with a mask with a diameter of 1 mm aperture being placed in front of electron detector. Thus, all threshold electrons are focused to go through the aperture, while the most energetic electrons deviate from the axis of flight tube and are blocked by the mask. However, a small part of energetic electrons with initial direction of emission along with the axis of flight tube can pass through the aperture and are assigned falsely as the threshold electrons. Thus, the false-coincidence measurement occurs inevitably to depress the resolution. A scheme was proposed by Sztáray and Baer to solve the problem [44]. Two detectors of multichannel plate were used to collect electrons, and one was placed just behind the aperture to measure the electrons flying along the axis while the other was settled off-center to collect the energetic electrons. Based on the hypothesis of isotropic electron emission in laboratory frame, the fraction of the false threshold electrons in the signals of the center detector could be estimated by the area ratio of two detectors. Therefore, the true TPES can be obtained with an improved energy resolution by subtracting the energetic electrons and normalizing by photon flux.

Generally, the weaker the extractor electric field is, the better the electron energy resolution is. However, a too weak extraction field may cause a very low collection efficiency of ion. Thus, a moderate-intensity extrac-

DOI:10.1063/1674-0068/32/cjcp1811257

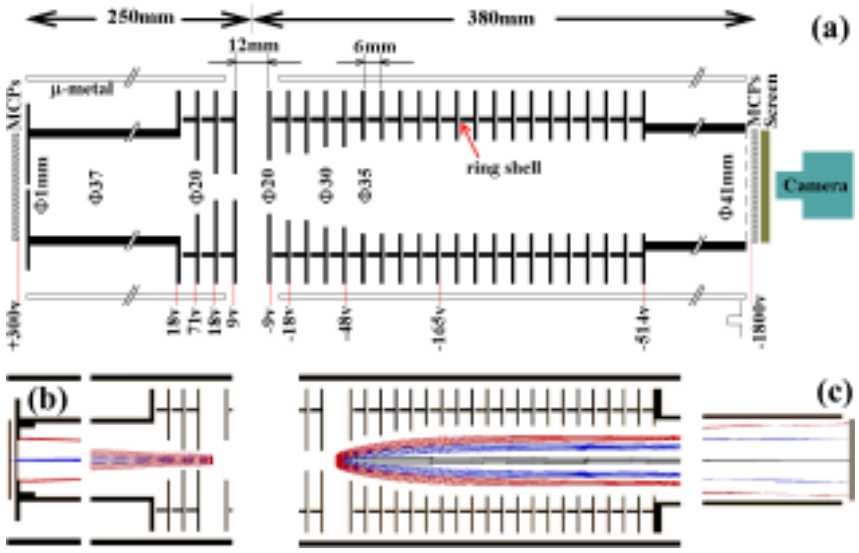

FIG. 2 (a) Geometric diagram of the velocity focusing optics and dual TOF tubes in the TPEPICO imaging spectrometer at HLS, (b) simulated trajectories of the threshold (in blue) and 50 meV (in red) energetic electrons, (c) simulated trajectories of ions with zero (in black), 0.3 eV (in blue), and 0.8 eV (in red) kinetic energy. In all simulations above, the extraction field is 15 V/cm. Reproduced with permission from Tang *et al.* [27]. Copyright 2009 American Institute of Physics.

tion field becomes primary when designing a TPEPICO setup. In the TPEPICO setup at HLS, a moderate electric field (typically 15 V/cm) has been usually applied to extract the charged particles with satisfying collection efficiency. Both the electrons and ions are pushed out of the photoionization region in the opposite directions, and the velocity focusing is achieved simultaneously for them under the action of the "soft focus lens" [30]. As shown in FIG. 2, a VMI field is used for ion image with 25 homocentric electrodes. Similar to Lin's design [30], a lens behind the extraction field is added to reduce the expanded ion packet under the soft focus condition. Whilst, a special retarding focus field is designed to prolong the flight time of electron. Under the same extraction field the energetic electrons expand from a few tens to a few hundred nanoseconds. Thus, the false-coincidence counting rate is evidently reduced at least tenfold, and the energy resolution of threshold electron is further improved.

With the double VMI design, the KERD and angular distribution of fragment ions can be directly measured. The resolving power of the released kinetic energy in dissociation, $\Delta E_{\rm tran}/E_{\rm tran}$, was determined to be ~2.4% [27], which was high enough to distinguish the vibrational populations of fragment ions. In this case, the dissociation dynamics of specific state-selected ions can be investigated with satisfying resolving power. Following the strategy, SLS [42] and SOLEIL [43] severally built the double VMI TPEPICO instruments recently. Although the reported electron energy resolution and the coincident counting rate were higher than those at HLS, their ion kinetic energy resolving powers are still needed to be improved.

In summary, several types of experiment can be performed by using the TPEPICO imaging spectrometer, *e.g.* MS-TPES of molecules, dissociative photoionization dynamics from TPEPICO imaging. From these measurements, not only the IE, D_0 and AP_0 values can be accurately determined, but also the detailed dynamics of dissociative photoionization may be obtained.

III. DISSOCIATION OF MOLECULAR ION IN SPECIFIC QUANTUM STATE

A. Appearance potential (AP_0) of fragment and dissociation energy (D_0)

D_0 and AP_0 are the key dynamic parameters to judge the major chemical routines in a complex system. Generally, their accurate measurement in gas phase is based on the thermodynamic cycle diagram in FIG. 3 [45]. Through photoionization with tunable VUV photon, the molecular ions in specific quantum state can be produced. If $AP_0(A^+/AB)$ is accurately obtained, the $D_0(A^+\text{-}B)$ value of molecular ion can be calculated as $D_0(A^+\text{-}B)=AP_0(A^+/AB)-IE(AB)$. Similarly, the dissociation energy of neutral molecule, D_0(A-B), equals to $AP_0(A^+/AB)$ minus $IE(A^+)$.

In the early experiments, AP_0 was estimated by fitting PIE curves of fragment [46]. According to the influence of thermal-distributed internal energy of neutral molecules, the Frank-Condon factor of photoionization and the kinetic shift, the fitted AP_0 values were of low accuracy. An upgraded acquisition of AP_0 is to fit the breakdown diagram, which shows the photon-energy de-

DOI:10.1063/1674-0068/32/cjcp1811257

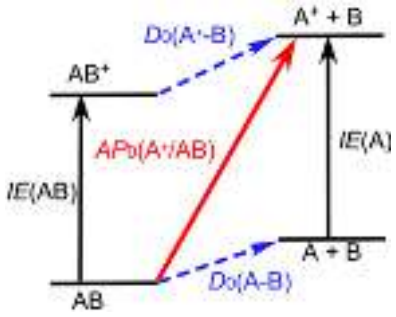

FIG. 3 Thermodynamic cycle diagram of gaseous molecule, based on the dissociative photoionization.

pendence of abundances of parent and fragment ions. With the increase of photon-energy around AP_0, the intensity of parent ion gradually reduces to zero, while the fragment ion appears and enhances. With a hypothesis of statistical unimolecular dissociation, the Maxwell-Boltzmann thermal distribution is assumed for the initial internal energy distribution of the dissociating ion. If there are multi-channels in the unimolecular dissociation, the branching ratio of specific fragment is proportional to the micro-canonical rate constant $k(\epsilon)$ of the corresponding channel, which can be calculated with the RRKM theory as Eq.(4) [47−49].

$$k(\epsilon) = \frac{\sigma \cdot N^{\neq}(\epsilon - \epsilon_0)}{h\rho(\epsilon)} \tag{4}$$

where $N^{\neq}(\epsilon-\Delta\epsilon_0)$ is the number of states of transition state at excess energy of $\epsilon-\Delta\epsilon_0$, $\rho(\epsilon)$ is the density of states of molecular ion, h is Planck's constant, and σ is the symmetry of the reaction coordinate. Thus, based on the computed vibrational frequencies and rotational constants of molecular ion and transition states, the $AP_0(A^+/AB)$ value can be obtained by fitting the breakdown diagram and reproducing the fractional ion abundances with the Eqs.(5)−(8) [50, 51].

For $h\nu$ <AP:

$$S_{\text{parent}}(h\nu) = \int_0^{\text{AP}_0-h\nu} P(\epsilon)\mathrm{d}\epsilon \tag{5}$$

$$S_{\text{daughter}}(h\nu) = \int_{\text{AP}_0-h\nu}^{\infty} P(\epsilon)\mathrm{d}\epsilon \tag{6}$$

For $h\nu$>AP:

$$S_{\text{parent}}(h\nu) = 0 \quad \text{and} \quad S_{\text{daughter}}(h\nu) = 1 \tag{7}$$

$$P(\epsilon) \propto \rho(\varepsilon)\mathrm{e}^{-\epsilon/(k_{\mathrm{B}}T)} \tag{8}$$

where $S_{\text{parent}}(h\nu)$ and $S_{\text{daughter}}(h\nu)$ are the intensity of parent and daughter ions in mass spectra, $P(\epsilon)$ is the internal energy distribution of neutral molecules.

As mentioned above, the temperature of molecular ions in photoionization is necessary to fit the breakdown diagram. Usually, the room temperature is optionally used although it is undefined due to Frank-Condon transition. Therefore, the fitted $AP_0(A^+/AB)$ value is expected with a certain amount of error, especially for those direct dissociation with a very fast rate.

In some cases, the dissociation may occur rapidly, and thus the lifetime of parent ion is not enough to complete the intramolecular vibrational distribution (IVR). Thus, internal energy of molecular ions is not thermally distributed. The highly symmetric molecules, *e.g.* CF_4, SF_6 and SeF_6 are the typical examples. Due to the unstable electronic ground states, the molecular ions directly dissociate along X−F (X=C, S, Se) bond rupture upon ionization. In this case, no abundance of parent ion exists in the breakdown curves, and hence the $AP_0(A^+/AB)$ value can not be obtained from the fitting method.

Taking CF_4 as an example, the electronic configuration of neutral CF_4 is $(3a_1)^2(2t_2)^6(4a_1)^2(3t_2)^6(1e)^4(4t_2)^6(1t_1)^6$. When an electron is removed from the outermost orbit ($1t_1$), the molecular ion $CF_4{}^+$ in the ground state, X^2T_1, is produced and quickly dissociated to produce $CF_3{}^+(X^1A_1)$ fragment ion and $F(^2P)$ atom. Therefore, only the upper limit of $AP_0(CF_3{}^+/CF_4)$ could be estimated from the released kinetic energy by analyzing the TOF profile of $CF_3{}^+$ in previous experiments [52]. Fortunately, the $AP_0(CF_3{}^+/CF_4)$ value could be obtained by directly measuring the KERD of $CF_3{}^+$ with the TPEPICO VMI technique. At 15.98 eV (just beyond IE_0 of CF_4), the $CF_3{}^+$ fragment ion was observed in TPEPICO mass spectra [35]. Through recording the time-sliced image of $CF_3{}^+$ as shown in FIG. 4, the total KERD in dissociative photoionization was obtained. Moreover, the parallel anisotropic distribution was consistent with the fast dissociation. Due to fast dissociation along the C−F bond rupture, the umbrella vibration ($v_2{}^+$=798.1 cm^{-1}) was dominantly excited. Taking into account the upper limit of $AP_0(CF_3{}^+/CF_4)$, the maximal $v_2{}^+$ quantum number of $CF_3{}^+(X^1A^1)$ was less than 10 at 15.98 eV, and the vibrational state population of $CF_3{}^+$ was assigned in FIG. 4 as well. From the maximal total KERD, the $AP_0(CF_3{}^+/CF_4)$ value of (14.71±0.02) eV could be calculated from the ground vibrational level as shown with an arrow in FIG. 4. This value exactly matched with the recent high-level quantum chemical calculation [53].

B. Vibrationally dependent dissociation of molecular ion

Since the double VMI is successfully combined with TPEPICO, the KERD and angular distribution of fragment ion can be directly obtained. Through gating the ion signal with ca. 40 ns, only those ions ejected perpendicularly to the extraction axis were collected for the time-sliced images [22]. Thus, the signal from a single dissociation reaction might appear only as a narrow ring in images. Benefiting from the high resolution of kinetic energy in VMI, we can get detailed information of dissociative photoionization.

DOI:10.1063/1674-0068/32/cjcp1811257

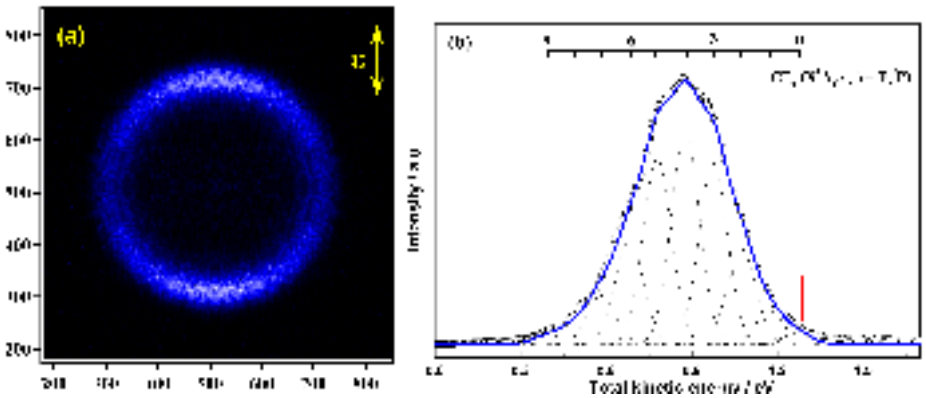

FIG. 4 Time-sliced TPEPICO velocity map image of CF_3^+ fragment and the corresponding total kinetic energy released distributions in dissociative photoionization of CF_4 at 15.98 eV. Reproduced with permission from Tang *et al.* [35]. Copyright 2013 American Institute of Physics.

Usually due to high density of states, dissociation of large polyatomic ions in the low-lying electronic states is statistical, which is described in terms of well-established statistical models. However, some large ions can dissociate directly on the repulsive potential energy surfaces of electronically excited states, and thus the relatively large translational energy is released and exceeds the prediction of statistical model. In contrast to large polyatomic ions, most of di- or tri-atomic ions show the non-statistical behavior owing to their sparse vibrational levels. Therefore, the vibrationally dependent dissociation of these ions can be observed in experiments. As a result, the fragment products formed from specific vibrational levels can be identified too by measuring the KERD in dissociative photoionization.

In the dissociative photoionization of N_2O at a photon range of 19.95−20.65 eV, a typical vibrationally dependence of dissociation dynamic was observed [31, 36]. Three vibronic levels of $C^2\Sigma^+$ ionic state, C(0, 0, 0), C(1, 0, 0) and C(0, 0, 1), were prepared in this energy range, where (v_1^+, v_2^+, v_3^+) were the quantum numbers of symmetric, bending and asymmetric vibrations, respectively. As shown in FIG. 5, two rings can be found in the TPEPICO images of NO^+ fragment, corresponding to the two dissociation channels involved in the dissociation. The inner ring is assigned to the higher dissociation channel of $NO^+(X^1\Sigma^+)$+N(^{2}P) and has a stronger intensity than that of the outer ring. With the aid of theoretical calculations, the NO^+ formation mechanism in the dissociation of $N_2O^+(C^2\Sigma^+)$ is summarized in Eq.(9) and Eq.(10) as well.

$$\begin{aligned} N_2O^+(C^2\Sigma^+) &\rightarrow N_2O^+(B^2\Pi) \\ &\rightarrow NO^+(X^1\Sigma^+, v^+) + N(^2P) \end{aligned} \quad (9)$$

or

$$\begin{aligned} &N_2O^+(C^2\Sigma^+) \rightarrow N_2O^+(B^2\Pi) \\ &\rightarrow^2 \Sigma^- \text{or } ^2\Delta \rightarrow NO^+(X^1\Sigma^+, v^+) + N(^2D) \end{aligned} \quad (10)$$

It was worth noting that the asymmetric vibration of $C^2\Sigma^+$ ionic state efficiently promoted dissociation possibility along the lowest channel of $NO^+(X^2\Sigma^+)$+N(^{2}D). According to the above dissociation mechanism, the vibrational dependence could be understood because the asymmetric vibration benefits the coupling from $B^2\Pi$ to the linear repulsive $^2\Sigma^-$ (or $^2\Delta$) ionic state.

Vibrational specific dissociation was also observed in dissociative photoionization of O_2 via the $B^2\Sigma_g^-$ ionic state [32, 34]. By ionizing with a VUV energy range of 20.1−21.1 eV, the O_2^+ ions were prepared in $B^2\Sigma_g^-$ (v^+=0−6) and $^2\Sigma_u^-$(v^+=0−7) states, where the latter was noted as a "optical dark" state due to forbidden transition from the ground ionic state. According to two energy-allowed dissociation channels of $O^+(^4S)$+O(^{3}P) and $O^+(^4S)$+O(^{1}D), the TPEPICO images of O^+ fragment showed a structure of two rings in FIG. 6 when the quantum number v^+ equaled to 4 and 6.

The outer narrow ring is attributed to the fragment produced along the lowest dissociation channel of $O^+(^4S)$+O(^{3}P), while the inner wide ring is contributed by the other decomposition pathway of $O^+(^4S)$+O(^{1}D). It is interesting to realize that the dissociation along the higher energy dissociation channel disappears at the $B^2\Sigma_g^-(v^+=5)$ state, although the internal energy of parent ion is higher than the dissociation limit.

As suggested by previous high-level calculations, the O(^{1}D) fragment was produced from $O_2^+(B^2\Sigma_g^-)$ via coupling to a repulsive $2^4\Pi_g$ state. The calculated intersection energy of $B^2\Sigma_g^-$ and $2^4\Pi_g$ states was located at near the v^+=6 level and higher than the experimental result of v^+=4. In fact, the v^+=4 level of $B^2\Sigma_g^-$ and the v^+=5 level of $^2\Sigma_u^-$ state are nearly degenerate, as shown in TPES or theoretical calculations. The dissociation of $^2\Sigma_u{}^-(v^+=5)$ could occur via coupling with the nearby $^4\Pi_u$ state and then producing $O^+(^4S)$+O(^{1}D),

DOI:10.1063/1674-0068/32/cjcp1811257

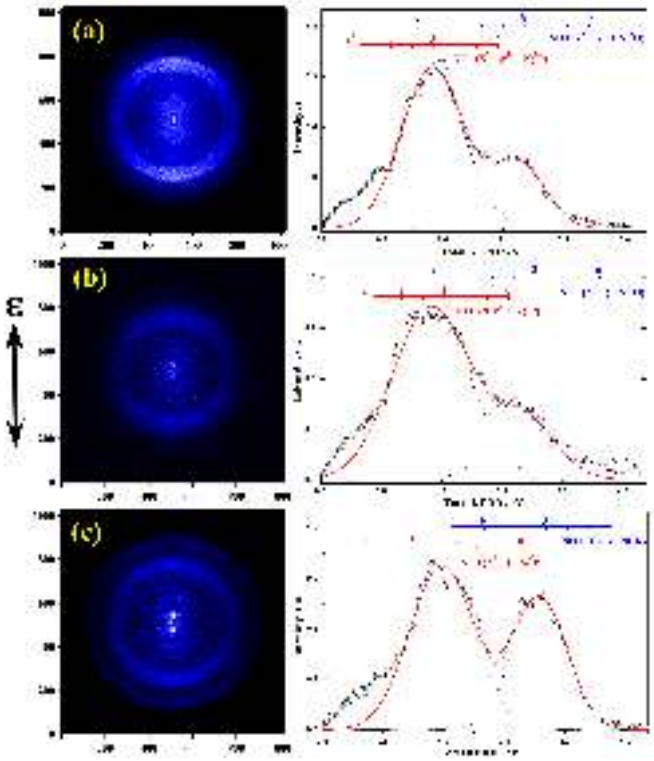

FIG. 5 Time-sliced TPEPICO velocity map images of NO^+ and the total kinetic energy released distributions in dissociation of N_2O^+ at various vibrational states of $C^2\Sigma^+$. The images are recorded at C(0, 0, 0), C(1, 0, 0) and C(0, 0, 1) vibronic levels, respectively, from top to bottom. Least-squares fitting of the total KERD curves with two Gaussian profiles are plotted with the solid line. Reproduced with permission from Tang *et al.* [31]. Copyright 2011 American Institute of Physics.

and their intersection energy is lower than the $B^2\Sigma_g^-$ (v^+=4) level. Thus, the O(^{1}D) fragment observed in experiment was the resonant dissociation product of $O_2{}^+(^2\Sigma_u^-, v^+=5)$, not from $B^2\Sigma_g^-(v^+=4)$ state. Moreover, when the ionization energy was increased to the higher v^+=5 level of $B^2\Sigma_g^-$, no incidental degeneration existed and thus no O(^{1}D) fragment was observed because the internal energy of $O_2{}^+$ was lower than the intersection of $B^2\Sigma_g^-$ and $2^4\Pi_g$ states. However, for $O_2{}^+(B^2\Sigma_g^-, v^+=6)$ ion, the O(^{1}D) fragment could reappear due to the internal energy beyond the intersection of $B^2\Sigma_g^-$ and $2^4\Pi_g$ states. Therefore, the optical dark ionic state, $^2\Sigma_u^-$, played a significant role in dissociation of $O_2{}^+$ within the excitation energy range.

C. Influence of electronic interaction on dissociation of molecular ion

The dissociation dynamics of polyatomic molecular ions with high symmetry is a hot topic and has attracted a great deal of attention in the past decades. The adiabatic and nonadiabatic effects, *e.g.* internal conversion and conical intersection, can be involved and show significant influences on the dissociation. In dissociative photoionization of CH_3Cl within the photon energy range of 11.0−18.5 eV [33], the C−Cl bond cleavage was observed for the CH_3Cl^+ ion in the lower electronically excited states, *e.g.* A^2A_1 and B^2E. The typical TPEPICO images of $CH_3{}^+$ fragment ion and their corresponding total KERD are displayed in FIG. 7.

As shown in FIG. 7, a series of homocentric rings were observed in the image of $CH_3{}^+$ fragment dissociated from $CH_3Cl^+(A^2A_1)$, but only a bright and structureless spot existed for dissociation of $CH_3Cl^+(B^2E)$, indicating that the different dissociation mechanisms happened for A^2A_1 and B^2E states. The A^2A_1 state is a typical repulsive state in Franck-Condon region as suggested by the high-level quantum chemical calculations [54]. When being prepared at A^2A_1 state, the C−Cl bond of CH_3Cl^+ will naturally break, and the structure of $CH_3{}^+$ moiety gradually changes from tetrahedral to plane configuration. Therefore, $CH_3{}^+$ fragment was observed to be excited at the mode of umbrella vibration. Moreover, the anisotropic parameter of the rings showed a dependence on the $v_2{}^+$ vibrational number, providing an experimental evidence of a shallow potential well along the C−Cl bond rupture predicted by theoretical calculation [54]. In addition, the proportion of average total released kinetic energy and available energy in dissociation was much lower than the value predicted by the classic "impulsive model", indicating that the partial relaxation of methyl group happened to change from the tetrahedral structure to planar during the impulsive period of dissociation.

Although the internal energy of B^2E ionic state was higher than that of A^2A_1, its dissociation along the Cl-loss channel was much slower. As the total KERD is shown with a Maxwell-Boltzmann profile in FIG. 7(b), a statistical dissociation was suggested for the C−Cl bond rupture of $CH_3Cl^+(B^2E)$ ion. The theoretical calculation confirmed the conclusion, because the B^2E state was bound and its Cl-loss process must happen via internal conversion to the high vibrational states of X^2E followed by statistical dissociation.

For the dissociation of another methyl halide ion, CF_3Cl^+, its mechanism becomes a little complex. By fitting the TOF mass peaks of fragment, dissociation of CF_3Cl^+ in different electronically excited states was briefly introduced but in query [55, 56]. Recently, dissociation of internal energy-selected CF_3Cl^+ ion was re-investigated in the photon energy region of 11.0−18.5 eV [39]. For the low-lying electronic states, A^2A_1 and B^2A_2 states, the TPEPICO images of the dominant fragment, $CF_3{}^+$, were recorded at 14.88 eV and 15.36 eV, and shown in FIG. 8. The A^2A_1 and B^2A_2 states overlap and comprise a wide peak in TPES, and the two photon energies locate within the peak. Thus, the CF_3Cl^+ parent ions prepared at the two pho-

DOI:10.1063/1674-0068/32/cjcp1811257

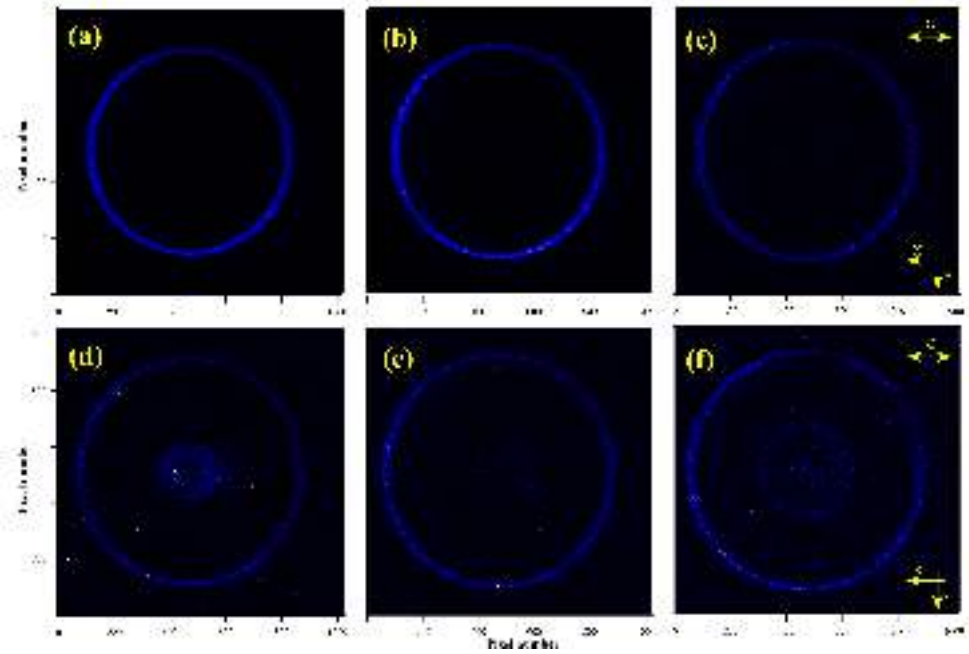

FIG. 6 Time-sliced TPEPICO images of O^+ fragment dissociated from $O_2{}^+(B^2\Sigma_g^-,\ v^+=1-6)$, respectively. Reproduced with permission from Tang *et al.* [32, 34]. Copyright 2011-2012 American Chemical Society.

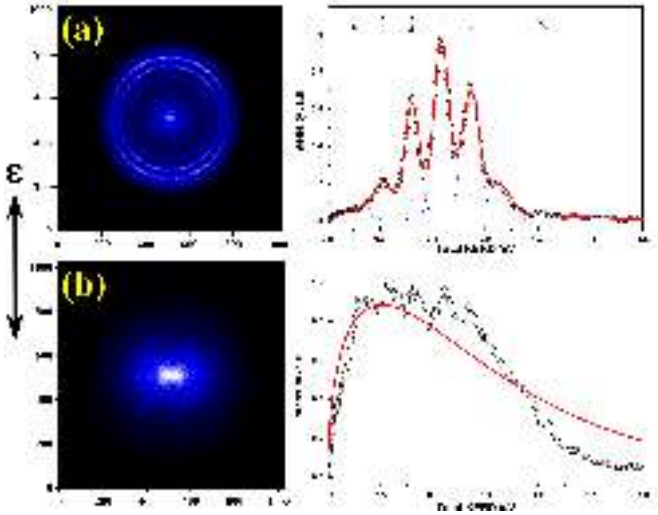

FIG. 7 Time-sliced TPEPICO velocity images of $CH_3{}^+$ fragment and the corresponding total kinetic energy released distributions in dissociation of CH_3Cl^+ ions, (a) A^2A_1 at 14.530 eV and (b) B^2E at 15.480 eV. Reproduced with permission from Tang *et al.* [33]. Copyright 2012 American Institute of Physics.

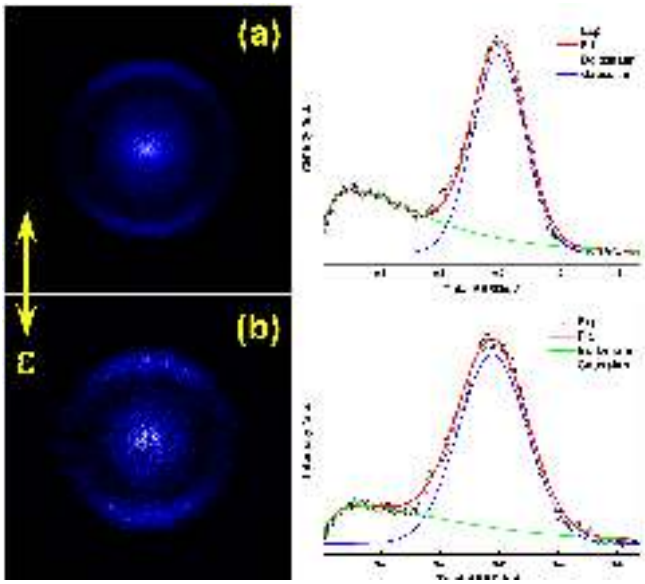

FIG. 8 Time-sliced TPEPICO velocity map images of $CF_3{}^+$ and the corresponding total kinetic energy released distributions in dissociation of CF_3Cl^+ ions, (a) A^2A_1 at 14.88 eV and (b) B^2E at 15.36 eV. Reproduced with permission from Tang *et al.* [39]. Copyright 2018 Royal Society of Chemistry.

ton energies should have both the contributions of the A^2A_1 and B^2A_2 states.

As we expected, two components existed in the images of FIG. 8, and the total KERD could be fitted very well with a Boltzmann- and one Gaussian-type curves. With the aid of theoretical calculations, the Cl-loss mechanism of CF_3Cl^+ at A^2A_1 and B^2A_2 states were clarified. The Boltzmann-type distribution in the total KERD was attributed to statistical dissociation of

DOI:10.1063/1674-0068/32/cjcp1811257

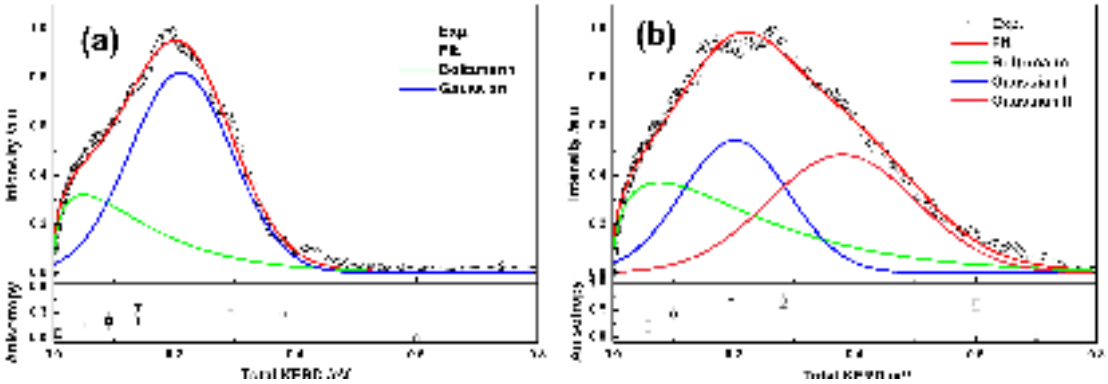

FIG. 9 The total kinetic energy released distributions in dissociation of $C_2H_3Cl^+$ in (a) B^2A'' at 13.14 eV and (b) C^2A' at 13.65 eV. Reproduced with permission from Wu *et al.* [38]. Copyright 2017 American Chemical Society.

the bound B^2A_2 component after internal conversion to the high vibrational level of the ground electronic state. The Gaussian one was contributed by the direct dissociation along the repulsive A^2A_1 state. As shown in the images, the non-statistical dissociation dominated. Moreover, the anisotropy parameters of the Gaussian component were close to 2, which was consistent with the character of repulsive A^2A_1 ionic state.

Another important electronic interaction, conical intersection, was found to play a significant role in dissociative photoionization of C_2H_3Cl [38]. The B^2A'' and C^2A' ionic states overlapped to a wide peak of 12.7−14.2 eV in TPES. At two typical photon energies, the time-sliced TPEPICO images of the unique fragment ion, $C_2H_3^+$, were recorded and the corresponding total KERDs were shown in FIG. 9. At 13.14 eV (mainly belonged to B^2A'' state), the total KERD showed a bimodal distribution consisting of Boltzmann- and Gaussian-type components, indicating a competition between statistical and non-statistical dissociation mechanisms. An additional Gaussian-type component was found in the KERD at 13.65 eV (in C^2A' state), a center of which was located at a lower kinetic energy (blue line in FIG. 9(b)). Although we could not assess the population fractions of C_2A' and highly vibrationally excited B^2A'' states at 13.65 eV, it should be emphasized that the new direct dissociation pathway was found and contributed by conical intersection between B^2A'' and C^2A'. In another words, the C^2A' state played an important role in dissociation dynamics of the nearby highly vibrationally excited B^2A'' state.

D. Identification of intermediates in complex chemical systems

Besides the above applications to investigate dissociation dynamics of energy-selected ions, TPEPICO technique has also been employed to probe products and intermediates in complex reaction systems, *e.g.* pyrolysis, flame and pulsed photolysis. MS-TPES is thought as a powerful analytical tool and has the advantage to identify free radicals and distinguish isomers [40].

In contrary to the smoothly changing PIE curves, each species exhibits sharp peaks in TPES and offers a greater selectivity [57]. MS-TPES becomes a preferred analytical and high-selective tool for detecting products of complex chemical systems, *e.g.* flow tube reactor [58, 59], pyrolysis [60−63], and combustion [64, 65].

The first successful attempt to determine the isomer mixture was performed at SLS using PEPICO [66]. A mixture of C_4H_6 (1,3-butadiene and 2-butyne, V/V=0.95/0.05) and C_5H_8 (cyclopentene, isoprene, 1-pentyne, and 1,4-pendadiene) was photoionized at a fixed photon energy, and the full PES ranging from 0 to 0.8 eV were analyzed. In FIG. 10(a), the black traces were the recorded PIE curves, where the presence of 2-butyne in the mixture could be shown by comparing the solid and dash lines. However, the appearing resonances of 2-butyne in TPES made its identification much more definitive. Moreover, FIG. 10(b) shows MS-TPES of m/z=54, where both butadiene and butyne are easily identifiable. Because only m/z=54 ions coincident to threshold photoelectron were collected in experiment, the spectral intensities were totally different from TPES of FIG. 10(a). The MS-TPES looked like a simple superposition of TPES of pure 1,3-butadiene (blue trace) and 2-butyne (green trace) with a certain weight. Above 9.5 eV, all spectral structures were dominantly contributed by those of 2-butyne, because the photoionization cross section of 2-butyne was much higher than that of 1,3-butadiene. Moreover, more vibrational resonances were observed besides the band origin as shown in FIG. 10(b), thus MS-TPES can provide more vibrational fingerprints for identifying isomers. With the aid of Franck-Condon calculation, the isomers can be distinguished and assigned efficiently in complex systems [67−69].

DOI:10.1063/1674-0068/32/cjcp1811257

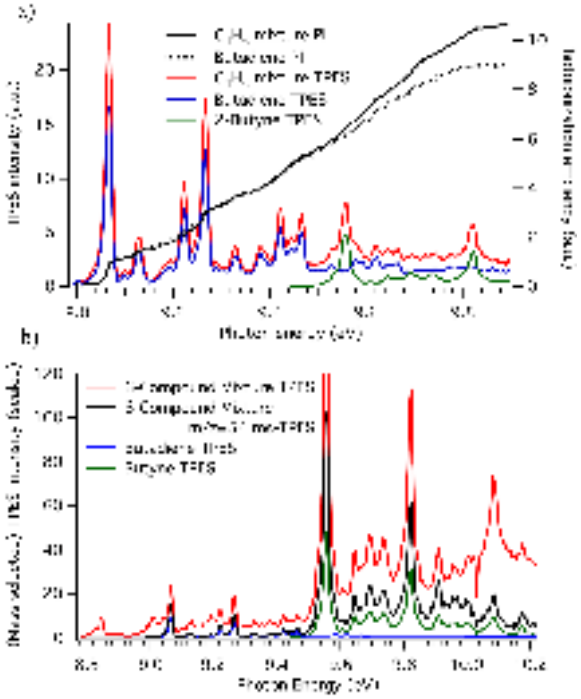

FIG. 10 (a) Threshold photoelectron spectrum of the 1,3-butadiene and 2-butyne mixture, as well as the TPES of the individual compounds (scaled). Here the PIE curves of the mixture and pure 1,3-butadiene are also shown for comparison. (b) Total TPES, m/z=54 MS-TPES of the mixture along with reference TPES of the two C_4H_6 isomers. Reproduced with permission from Bodi *et al.* [66]. Copyright 2011-2012 American Chemical Society.

IV. CONCLUSIONS AND FUTURE DIRECTIONS

As a state-of-the-art experimental approach, TPEPICO VMI has the advantage to investigate the dissociation dynamics of state-selected molecular ions. Especially, the utilization of the double VMI for both photoelectron and photoion has greatly improved the collection efficiency of the charged particles, the energy resolution of threshold electron and the resolving power of KERD in dissociation.

For polyatomic molecule, the fundamental molecular parameters, such as IE, D_0 and AP_0, can be accurately measured in TPEPICO experiments. The significant non-adiabatic quantum effects, like conical intersection and internal conversion, involved in the dissociation of ions, have been investigated. For the most organic molecular ions, the internal conversion from the highly excited electronic state to the ground electronic state is very fast due to the high density of states, and thus the dissociation of electronically excited states usually exhibits the statistical features on the potential energy surface of ground electronic state. But, some special ions, like $CF_4{}^+$ with an unstable ground state, still exhibit state-selected dissociation dynamics and the TPEPICO imaging has already demonstrated its ability on it.

Besides these applications presented in this review, another potential application of the coincidence technique is to study photo-induced ion-pair formation,

$$AB + h\nu \rightarrow \ A^+ + B^- \qquad (11)$$

This special fragmentation pathway occurs in the excitation energy of IE_0 to AP_0, and thus it causes the A^+ fragment appear below the lowest dissociation channel of molecular ion, $AB^+ \rightarrow A^+ + B$. Under photolysis with the tunable VUV light, we can straight detect the negative fragment ion by using electron optics, and record the velocity map images of coincident cations and anions with the double VMI. The high resolution KERD and angular distribution of the positive and negative fragments can be measured and correlated directly. Thus, the detailed dynamic information of ion-pair formation of polyatomic molecule can be obtained.

TPEPICO also shows another important application to probe complex reaction systems during the past years. The MS-TPES has been thought as a powerful tool for identifying intermediates. It shows tremendous potential for quantitative and isomer-specific analysis of complex systems. Not only the fundamental parameters like IE_0 and AP_0, but also the vibrational signatures are observed in MS-TPES. Therefore, it provides higher selectivity compared to the traditional PIE, and has been successfully applied in complex chemical systems, *e.g.* flow tube reactor, pyrolysis and combustion, when combining with the VUV synchrotron radiation.

Recently, the MS-TPES was used for detection of catalytic intermediates at the VUV beamline of SLS [70, 71]. A temperature-controlled products-type (TAP) [72] pyrolysis reactor was combined to the imaging PEPICO spectrometer (iPEPICO). In the catalytic pyrolysis of guaiacol within a temperature range of 400−500 °C [70]. The MS-TPES of the most relevant species at m/z=66, 78, 80, and 92, were recorded, respectively. According to Franck-Condon simulations, the m/z=66 peak (C_5H_6) was readily identified as cyclopentadiene (c-C_5H_6). The onset in MS-TPES of the m/z=78, C_6H_6, was lower than IE_0 of benzene (9.244 eV) [73], indicating the existence of another isomer. The fulvene (c-C_5H_4=CH_2) was proposed to be the dominant contributor. For the m/z=80 ion, the observed vibrational structure indicated that it should belong to three methyl-cyclopentadiene (c-C_5H_5−CH_3) isomers instead of antiaromatic cyclopentadienone (c-C_5H_4=O, m/z=80) suggested in previous study [74].

However, it is worth noting that the TPEPICO imaging also has a couple of limitations. As mentioned above, the signal-to-noise ratio may be too worse to record the satisfying images of fragment ions when the photoionization cross section to yield threshold photoelectrons is small. The case occurs occasionally for the molecular ion in a highly excited electronic state. More importantly, there is a hypothesis without taking into

DOI:10.1063/1674-0068/32/cjcp1811257

account the direct three-body dissociative photoionization to produce an electron, A^+ and B fragments, due to the lack of a satisfying theoretical method to deal with the photoionization dynamics of polyatomic molecules. Actually, all the dissociative photoionization processes in the examples mentioned above are artificially thought to occur indirectly as the ionization followed by dissociation of the energy- or state-selected ions. Fortunately, it is consistent with the experimental data because the overall process is far slower than the direct three-body mechanism, based on the moderate anisotropy parameters.

In summary, the multiplex advantages of double imaging detection of electrons and ions in PEPICO measurement make it attract more and more attention. We believe, with the further improvement of false coincidence suppression, TPEPICO VMI approach will become a truly universal and powerful tool to analyze intermediates and isomers in the near future.

V. ACKNOWLEDGMENTS

The authors sincerely appreciate Profs. Kopin Liu and Cheuk Yiu Ng for their fruitful discussions and advices when designing the double VMI setup. The works were supported by the Instrument Developing Project of the Chinese Academy of Sciences (No.YZ200763), the National Natural Science Foundation of China (No.21027005, NO.21573210 and No.21873089), the National Key Research and Development program (No.2016YFF0200502), and the National Key Basic Research Foundation (No.2013CB834602). Xiang-kun Wu thanks the Chinese Postdoctoral Foundation (No.2018M632535). Xiao-guo Zhou also appreciates Dr. Andras Bodi for sending us the high resolution copy of FIG. 10.

[1] X. M. Yang, T. K. Minton, and D. H. Zhang, Science **336**, 1650 (2012).
[2] C. Y. Ng, Annu. Rev. Phys. Chem. **53**, 101 (2002).
[3] H. F. Xu, Y. Guo, Q. F. Li, Y. Shi, S. L. Liu, and X. X. Ma, J. Chem. Phys. **121**, 3069 (2004).
[4] C. H. Chang, C. Y. Luo, and K. Liu, J. Phys. Chem. A **109**, 1022 (2005).
[5] H. Wang, X. G. Zhou, S. L. Liu, B. Jiang, and D. X. Dai, J. Chem. Phys. **132**, 244309 (2010).
[6] C. M. Zhang, J. L. Li, Q. Zhang, Y. Chen, C. S. Huang, and X. M. Yang, Phys. Chem. Chem. Phys. **14**, 2468 (2012).
[7] B. Brehm and E. von Puttkamer, Z. Naturforsch A: Phys. Sci. **22**, 8 (1967).
[8] G. R. Parr and J. W. Taylor, Rev. Sci. Instrum. **44**, 1578 (1973).
[9] T. Baer, Annu. Rev. Phys. Chem. **40**, 637 (1989).
[10] C. A. Taatjes, N. Hansen, D. L. Osborn, K. Kohse-Höinghaus, T. A. Cool, and P. R. Westmoreland, Phys. Chem. Chem. Phys. **10**, 20 (2008).
[11] F. Qi, Proc. Combust. Inst. **34**, 33 (2013).
[12] L. Belau, K. R. Wilson, S. R. Leone, and M. Ahmed, J. Phys. Chem. A **111**, 10075 (2007).
[13] K. B. Bravaya, O. Kostko, M. Ahmed, and A. I. Krylov, Phys. Chem. Chem. Phys. **12**, 2292 (2010).
[14] O. Kostko, K. Bravaya, A. Krylov, and M. Ahmed, Phys. Chem. Chem. Phys. **12**, 2860 (2010).
[15] T. A. Field and J. H. Eland, Meas. Sci. Technol. **9**, 922 (1998).
[16] A. S. Werner and T. Baer, J. Chem. Phys. **62**, 2900 (1975).
[17] D. Villarejo, R. R. Herm, and M. G. Inghram, J. Chem. Phys. **46**, 4995 (1967).
[18] T. Baer, W. B. Peatman, and E. Schlag, Chem. Phys. Lett. **4**, 243 (1969).
[19] P. Hatherly, M. Stankiewicz, K. Codling, J. Creasey, H. Jones, and R. Tuckett, Meas. Sci. Technol. **3**, 891 (1992).
[20] R. Hall, A. McConkey, K. Ellis, G. Dawber, L. Avaldi, M. MacDonald, and G. King, Meas. Sci. Technol. **3**, 316 (1992).
[21] T. Baer and Y. Li, Int. J. Mass Spectrom. **219**, 381 (2002).
[22] G. A. Garcia, H. Soldi-Lose, and L. Nahon, Rev. Sci. Instrum. **80**, 023102 (2009).
[23] W. Wiley and I. H. McLaren, Rev. Sci. Instrum. **26**, 1150 (1955).
[24] R. Vasudev, R. Zare, and R. Dixon, J. Chem. Phys. **80**, 4863 (1984).
[25] D. Seccombe, R. Chim, G. Jarvis, and R. Tuckett, Phys. Chem. Chem. Phys. **2**, 769 (2000).
[26] K. M. Weitzel and J. Mähnert, Int. J. Mass Spectrom. **214**, 175 (2002)
[27] X. F. Tang, X. G. Zhou, M. L. Niu, S. L. Liu, J. D. Sun, X. B. Shan, F. Y. Liu, and L. S. Sheng, Rev. Sci. Instrum. **80**, 113101 (2009).
[28] A. T. Eppink and D. H. Parker, Rev. Sci. Instrum. **68**, 3477 (1997).
[29] D. Townsend, M. P. Minitti, and A. G. Suits, Rev. Sci. Instrum. **74**, 2530 (2003).
[30] J. J. Lin, J. Zhou, W. Shiu, and K. Liu, Rev. Sci. Instrum. **74**, 2495 (2003).
[31] X. F. Tang, M. L. Niu, X. G. Zhou, S. L. Liu, F. Y. Liu, X. B. Shan, and L. S. Sheng, J. Chem. Phys. **134**, 054312 (2011).
[32] X. F. Tang, X. G. Zhou, M. L. Niu, S. L. Liu, and L. S. Sheng, J. Phys. Chem. A **115**, 6339 (2011).
[33] X. F. Tang, X. G. Zhou, M. M. Wu, S. L. Liu, F. Y. Liu, X. B. Shan, and L. S. Sheng, J. Chem. Phys. **136**, 034304 (2012).
[34] X. F. Tang, X. G. Zhou, M. M. Wu, Y. Cai, S. L. Liu, and L. S. Sheng, J. Phys. Chem. A **116**, 9459 (2012).
[35] X. F. Tang, X. G. Zhou, M. M. Wu, Z. Gao, S. L. Liu, F. Y. Liu, X. B. Shan, and L. S. Sheng, J. Chem. Phys. **138**, 094306 (2013).
[36] X. F. Tang, X. G. Zhou, B. L. Qiu, S. L. Liu, F. Y. Liu, X. B. Shan, and L. S. Sheng, J. Electron Spectrosc. Relat. Phenom. **196**, 43 (2014).
[37] X. F. Tang, X. G. Zhou, Z. F. Sun, S. L. Liu, F. Y. Liu, L. S. Sheng , and B. Yan, J. Chem. Phys. **140**, 044312 (2014).
[38] X. K. Wu, M. M. Wu, X. F. Tang, X. G. Zhou, S. L. Liu, F. Y. Liu, and L. S. Sheng, J. Phys. Chem. A **121**,

4743 (2017).
[39] X. K. Wu, G. Q. Tang, H. H. Zhang, X. G. Zhou, S. L. Liu, F. Y. Liu, L. S. Sheng, and B. Yan, Phys. Chem. Chem. Phys. **20**, 4917 (2018).
[40] O. Kostko, B. Bandyopadhyay, and M. Ahmed, Annu. Rev. Phys. Chem. **67**, 19 (2016).
[41] T. Baer and R. P. Tuckett, Phys. Chem. Chem. Phys. **19**, 9698 (2017).
[42] A. Bodi, P. Hemberger, T. Gerber, and B. Sztáray, Rev. Sci. Instrum. **83**, 083105 (2012).
[43] G. A. Garcia, B. K. Cunha de Miranda, M. Tia, S. Daly, and L. Nahon, Rev. Sci. Instrum. **84**, 053112 (2013).
[44] B. Sztáray and T. Baer, Rev. Sci. Instrum. **74**, 3763 (2003).
[45] Y. R. Luo, *Comprehensive Handbook of Chemical Bond Energies*, Boca Raton: CRC press (2007).
[46] C. Y. Ng, Adv. Chem. Phys. **52**, 263 (1982).
[47] O. K. Rice and H. C. Ramsperger, J. Am. Chem. Soc. **49**, 1617 (1927).
[48] O. K. Rice and H. C. Ramsperger, J. Am. Chem. Soc. **50**, 617 (1928).
[49] R. A. Marcus and O. K. Rice, J. Phys. Chem. **55**, 894 (1950).
[50] B. Sztáray, A. Bodi, and T. Baer, J. Mass Spectrom. **45**, 1233 (2010).
[51] T. Baer, *Gas Phase Ion Chemistry*, New York: Academic, (1979).
[52] R. Chim, R. Kennedy, R. Tuckett, W. Zhou, G. Jarvis, C. Mayhew, D. Collins, and P. Hatherly, Surf. Rev. Lett. **9**, 129 (2002).
[53] A. Bodi, Á. Kvaran, and B. Sztáray, J. Phys. Chem. A **115**, 13443 (2011).
[54] H. W. Xi, M. B. Huang, B. Z. Chen, and W. Z. Li, J. Phys. Chem. A **109**, 4381 (2005).
[55] I. Powis, Mol. Phys. **39**, 311 (1979).
[56] J. C. Creasey, D. M. Smith, R. P. Tuckett, K. R. Yoxall, K. Codling, and P. A. Hatherly, J. Phys. Chem. **100**, 4350 (1996).
[57] J. M. Dyke, J. Chem. Soc., Faraday Trans. **283**, 69 (1987).
[58] D. Schleier, P. Constantinidis, N. Faßheber, I. Fischer, G. Friedrichs, P. Hemberger, E. Reusch, B. Sztáray, and K. Voronova, Phys. Chem. Chem. Phys. **20**, 10721 (2018).
[59] K. Voronova, K. M. Ervin, K. G. Torma, P. Hemberger, A. Bodi, T. Gerber, D. L. Osborn, and B. Sztáray, J. Phys. Chem. Lett. **9**, 534 (2018).
[60] Y. P. Zhu, X. K. Wu, X. F. Tang, Z. Y. Wen, F. Y. Liu, X. G. Zhou, and W. J. Zhang, Chem. Phys. Lett. **664**, 237 (2016).
[61] H. Dossmann, G. A. Garcia, L. Nahon, B. K. de Miranda, and C. Alcaraz, J. Chem. Phys. **136**, 204304 (2012).
[62] P. Hemberger, A. J. Trevitt, E. Ross, and G. da Silva, J. Phys. Chem. Lett. **4**, 2546 (2013).
[63] M. Lang, F. Holzmeier, P. Hemberger, and I. Fischer, J. Phys. Chem. A **119**, 3995 (2015).
[64] P. Oßwald, P. Hemberger, T. Bierkandt, E. Akyildiz, M. Köhler, A. Bodi, T. Gerber, and T. Kasper, Rev. Sci. Instrum. **85**, 025101 (2014).
[65] J. Krüger, G. A. Garcia, D. Felsmann, K. Moshammer, A. Lackner, A. Brockhinke, L. Nahon, and K. Kohse-Höinghaus, Phys. Chem. Chem. Phys. **16**, 22791 (2014).
[66] A. Bodi, P. Hemberger, D. L. Osborn, and B. Sztáray, J. Phys. Chem. Lett. **4**, 2948 (2013).
[67] P. Hemberger, A. J. Trevitt, T. Gerber, E. Ross, and G. da Silva, J. Phys. Chem. A **118**, 3593 (2014).
[68] P. Hemberger, G. da Silva, A. J. Trevitt, T. Gerber, and A. Bodi, Phys. Chem. Chem. Phys. **17**, 30076 (2015).
[69] S. Y. Liang, P. Hemberger, N. M. Neisius, A. Bodi, H. Grützmacher, J. Levalois-Grützmacher, and S. Gaan, Chem. Eur. J. **21**, 1073 (2015).
[70] P. Hemberger, V. B. Custodis, A. Bodi, T. Gerber, and J. A. van Bokhoven, Nat. Commun. **8**, 15946 (2017).
[71] V. Paunović, P. Hemberger, A. Bodi, N. López, and J. Prez-Ramírez, Nat. Catal. **1**, 363 (2018).
[72] J. T. Gleaves, J. Ebner, and T. Kuechler, Cat. Rev.: Sci. Eng. **30**, 49 (1988).
[73] G. Nemeth, H. Selzle, and E. Schlag, Chem. Phys. Lett. **215**, 151 (1993).
[74] A. M. Scheer, C. Mukarakate, D. J. Robichaud, M. R. Nimlos, and G. B. Ellison, J. Phys. Chem. A **115**, 13381 (2011).

DOI:10.1063/1674-0068/32/cjcp1811257